A Nonlinear Cause for the seasonal Predictability Barrier of SST anomaly in the 2 tropical Pacific

Dakuan Yu[1], Meng Zhou[1], Chaoxun Hang[1], and De-Zheng Sun[2]

[1]Shanghai Jiao Tong University
[2]Fudan University

November 21, 2022

Abstract

The seasonal Predictability Barrier (PB) of Sea Surface Temperature Anomaly (SSTA) is characterized by a rapid loss of prediction skills at a specific season in dynamic models. To investigate whether this PB phenomenon is caused by the inherent nonlinearity of the air-sea coupled system that leads to chaos under certain conditions, a statistical method - Sample Entropy, was introduced to investigate the spatial-temporal distribution of the chaotic degree of SSTA time series in the tropic Pacific. The results showed that high chaotic values existed in Niño 3 and Niño 3.4 regions in April and May, and in Niño 4 region in May and June, which matched the PB timing previously reported in these regions. Furthermore, the chaotic signal moves westward from March to June longitudinally in the tropical Pacific, leading to a similar linear variation of PB timing along the longitude.

A Nonlinear Cause for the seasonal Predictability Barrier of SST anomaly in the tropical Pacific

Dakuan. Yu.[1], Meng. Zhou.[1], Chaoxun. Hang.[1], and De-Zheng. Sun.[2]

1 School of Oceanography, Shanghai Jiao Tong University, Shanghai, China.

2 Institute of Atmospheric Sciences, Fudan University, Shanghai, China.

Corresponding author: Meng. Zhou. (meng.zhou@sjtu.edu.cn)

Key Points:

- Sample Entropy method is utilized to study the nonlinearity of the seasonal Predictability Barrier of SSTA in the tropical Pacific
- The seasonal variations of the nonlinear regime of the air-sea coupled system are responsible for the Predictability Barrier
- Both the Predictability Barrier timing and peak chaotic month show linear variation along the longitude in the tropical Pacific.

Abstract

The seasonal Predictability Barrier (PB) of Sea Surface Temperature Anomaly (SSTA) is characterized by a rapid loss of prediction skills at a specific season in dynamic models. To investigate whether this PB phenomenon is caused by the inherent nonlinearity of the air-sea coupled system that leads to chaos under certain conditions, a statistical method - Sample Entropy, was introduced to investigate the spatial-temporal distribution of the chaotic degree of SSTA time series in the tropic Pacific. The results showed that high chaotic values existed in Niño 3 and Niño 3.4 regions in April and May, and in Niño 4 region in May and June, which matched the PB timing previously reported in these regions. Furthermore, the chaotic signal moves westward from March to June longitudinally in the tropical Pacific, leading to a similar linear variation of PB timing along the longitude.

Plain Language Summary

Accurate predictions of Sea Surface Temperature Anomaly (SSTA) in the tropical Pacific are in high demand. However, the dynamic models always lost their prediction skill of SSTA during a certain season, which is known as the seasonal Predictability Barrier (PB). This poor prediction has two different causes: one is the discrepancy in the model, which means that some critical physical processes are not well captured in the models; the other is the “Butterfly effect” or chaos, which will lead to the rapid growth of initial uncertainty in the models and make the air-sea coupled system inherently unpredictable. To investigate whether the PB phenomenon is an inherent character of the air-sea coupled system, a statistic method - Sample Entropy, is introduced to investigate the spatial-temporal distribution of the chaotic degree of SSTA time-series in the tropic Pacific. The results showed that the spatial-temporal distribution of the chaotic degree is consistent with that of the PB timing and indicate that the PB of SSTA is likely an inherent character of the air-sea coupled system. To overcome the PB of SSTA, more efforts need to be paid to improve the accuracy of the initial fields in the model in the tropical Pacific.

1 Introduction

The Sea Surface Temperature Anomalies (SSTA) in the Tropical Pacific Ocean (TPO) play significant roles in affecting the global climate (Wang & Ting, 2000; Castro et al., 2001; Marzban & Schaefer, 2001; Fereday et al., 2008; McKinnon et al., 2016). For instance, the interannual SSTA variability in the TPO, namely the El Niño phenomenon, strongly affects the climate (e.g., temperature, wind speed, precipitation, etc.) in East Asia (Gao et al., 2006; Wu et al., 2003, 2010; Yuan & Yang, 2012) and North America (Ropelewski & Halpert, 1986; Hu & Feng, 2012; Infanti & Kirtman, 2016), as well as the variabilities of sea ice extent and concentration in the Antarctic and Arctic regions (Yuan, 2004; Dash et al., 2013; Clancy et al., 2021). Accurate predictions of SSTA in TPO are crucial for mitigating the risks of extreme weather and political decision-making (Solow et al., 1998; Trenberth et al., 1998; Patt & Gwata, 2002; Pierce, 2002). Over the past years, six-month advanced predictions of SSTA have been achieved in the TPO through the ocean-atmosphere coupled models (Xue et al., 2013; Tang et al., 2018; Song et al., 2020). However, one-year prediction in advance is still challenged due to the so-called seasonal Predictability Barrier (PB) (Webster, 1995; Webster & Yang, 1992; van Oldenborgh et al., 2005; Jin et al., 2008; Tang et al., 2018), which is known as a rapid loss of prediction skills in most SSTA forecast models during certain seasons (Torrence & Webster, 1998).

The Predictability Barrier has been reported globally during various seasons. It has been found in spring in the eastern TPO (Duan & Wei, 2013), summer in the northern Pacific Ocean and central TPO (Duan & Wu, 2015; Ren et al., 2016), and winter in the Indian Ocean Dipole region (Liu et al., 2018). Even though enormous efforts have been dedicated to investigating the control mechanisms of the PB of SSTA, there is still a need for more results for a better understanding of the nature of PB (McPhaden, 2003; Li & Ling, 2009; Hu et al., 2014). Some researchers suggested that the PB of SSTA was triggered by the stochastic noise in the ocean and atmosphere (Torrence & Webster 1998; Lopez & Kirtman, 2014; Levine & McPhaden 2015; Mukhin et al., 2021). Others believed that the initial errors of SSTA in the dynamic models were responsible for the PB of SSTA (Lau & Yang, 1996; Moore, 1999; Samelson & Tziperman 2001; Zheng & Zhu 2010; Larson & Kirtman, 2015; Hou et al., 2019). However, it is unclear why the initial error in models grows at the quickest rate in these seasons, as the growth of the initial error in models can be caused by two different factors. One is the discrepancy in dynamic models - the missing of some key physical processes compared with the real world (Collins et al. 2002). The other is due to the nonlinearity of the system, which can cause small initial errors to grow exponentially if the system is in a chaotic regime (Lorenz 1963). The latter was suggested by Samelson and Tziperman (2001) as a possible cause for the PB of SSTA in the TPO, but their study is based on the numerical model. Hence, whether the model error will affect their results is unclear. Moreover, previous studies have uncovered the multiple regimes of the coupled ocean-atmosphere system in the TPO owing to nonlinearity, and suggested that ENSO results fundamentally from the instability of these dynamic regimes (Sun 1997; Liang et al. 2012; Liang et al. 2017; Hua et al. 2019). Hence, the inherent nonlinearity in the coupled system as a cause for the PB of SSTA remains to be established.

Recent progress in time series analysis of the nonlinear systems has raised the possibility to settle this issue, as these statistical techniques allow us to determine the dynamic regime of the observed coupled system through analyzing observations (Fraedrich, 1987; Kantz & Schreider, 2004; Bradley & Kantz, 2015 among others). Karamperidou et al. (2014) used the local Lyapunov Exponents to characterize the predictability of active and inactive periods of ENSO in a climate model, but they did not specifically address the causes for the seasonal PB of SSTA. Ding and Li (2007) proposed a Nonlinear Local Lyapunov Exponent (NLLE) method to study the mean error growth rate and predictability limit of chaotic systems. The general idea of the NLLE method is to calculate the difference between two analogs of the evolution pattern from the observed time series. If the difference between two analogous time series grows quickly, the error growth rate of the studied system is large. Utilizing the NLLE method, Li and Ding (2013) found that the initial errors grow quickly when the prediction was across the spring in the TPO and suggested that the spring PB might be intrinsic to the real air-sea coupled system. However, the seasonal mean error growth rate measured by the NLLE method was affected by the error from previous seasons. When the errors are initiated from different seasons, all these errors will grow quickly and reach a large value at first, and then have a quick growth rate in the spring (seen in Fig. 5 in Li and Ding (2013)). Therefore, using the NLLE method cannot determine unambiguously whether the rapid growth of errors in a certain season results from the inherent nonlinearity of the studied system or the errors of other seasons. Perhaps because of this reason, the NLLE method has not been widely used in the study of different systems, which has further cast doubt on the validity of this method in the study of the problem of the seasonal barriers for ENSO predictability.

To ensure that the inherent error originates solely from the time of interest, the Sample Entropy (SamEn) method (Richman & Moorman, 2000) was chosen to analyze the inherent error growth rate of SSTA in the entire TPO region and explore its relationship with the seasonal PB of SSTA. SamEn is the relative estimation of the sum of positive Lyapunov Exponents (Fraedrich, 1987; Pincus, 1991, 1995; Richman & Moorman, 2000), which can be taken as the degree of the chaos of dynamic systems (Wolff, 1992). The SamEn method concerns the error growth rate in the studied period, and the results are not affected by the errors from another period. The applicability of SamEn and its variations have been well examined in broad disciplines including physiological time-series analysis (Richman & Moorman, 2000; Lake et al. 2002; Eduardo Virgilio Silva & Otavio Murta, 2012), de-noising for hydrologic signals (Wang et al. 2014; Li et al. 2019), turbulent experimental data analysis (Kim 2021), and even the stock markets study (Shi & Shang, 2013).

2 Data

2.1 Data

Daily ocean temperature data from 1994 to 2015 is obtained from the HYCOM global daily snapshot 0Z 1/12 degree Global Ocean Forecasting System (GOFS) 3.1 reanalysis datasets (http://apdrc.soest.hawaii.edu/dods/public_ofes/HYCOM/GLBv0.08), which have been validated against observations with consistent results reported (Chassignet et al., 2007). The longitude resolution of the dataset is 0.08° between 0°E-360°E. The latitude resolution is 0.08° between 40°S-40°N and 0.04° between 40°N-90°N and 90°S-40°S. The number of vertical levels is 40. In the upper 12 m, there are 7 layers, and the vertical interval is about 2 m. Between 15m to 50m, 50m to 100m, and 150m to 400m, there are 8, 6, and 6 layers with the vertical interval of 5m, 10m, and 50m, respectively. The dataset contains the data between 1994–2015, which is the maximum time range of this HYCOM GOFS 3.1 dataset. In this study, the TPO is defined within the range of 10ºS-10ºN and 155ºE-90ºW. To reduce the computational cost, the horizontal grids of HYCOM datasets are interpolated into the same 2° longitude and 2° latitude grids. The finer grid than the 2° longitude and 2° latitude will not affect the results (the results are not shown). The longitude and latitude resolution of climatology data are 2° between 155°E-90°W and 10°S-10°N. The daily anomalous data are computed by removing the climatological mean annual cycle and trend from the SST data at each grid point.

The SSTA forecast data in dynamic models are from the North American Multi-Model Ensemble (NMME) dataset, which is the state-of-art coupled ensemble model to predict the SSTA variation in the TPO. It provides monthly retrospective forecasts (or hindcast) data with a maximum range between 1981 to 2018 (Kirtman et al. 2014). The NMME data set has been continuously evaluated and shows a good performance of region climate predictability (Barnston et al. 2019; Becker et al. 2020). The NMME model set contains twenty-nine different models, but only eight of them cover our study period, which is between 1994 to 2015. Hence, in this study, the hindcast results from these eight different dynamic models in the NMME model set were chosen to calculate the forecast error of SSTA in the TPO. The details of these eight different dynamic models can be found in Table S1. The SSTA forecast data are interpolated into the same 2° longitude and 2° latitude grids as the HYCOM reanalysis data. Forecast errors are defined as the difference between the forecast SSTA value and the observed HYCOM SSTA value.

2.2 Method

The SamEn method quantifies the self-similarity degree of a time series by examining the number of instances, that two subsequences in the time series are still similar when the length of subsequences increases. More details can be found in Delgado-Bonal and Marshak (2019).

For an arbitrary time-series data $H = \{H_n | H_1, H_2, H_3 \dots H_N\}$ of length N, the time series can be reconstructed to a subsequent matrix:

$$\Psi^m = \begin{bmatrix} H_1 & H_2 & \dots & H_m \\ H_2 & H_3 & \dots & H_{m+1} \\ \dots & \dots & \dots & \dots \\ H_{N-m} & H_{N-m+1} & \dots & H_{n-1} \end{bmatrix}, \quad (1)$$

which contains m columns and $N - m$ rows. m is the embedding dimension number (Richman & Moorman, 2000), which is the minimum time scale considered.

The subsequent vector Ψ_i^m is defined as a row in Ψ^m, which can be written as follows:

$$\Psi_i^m = \{H_i, H_{i+1} \dots H_{i+m-1}\} \qquad 1 \le i \le N - m. \quad (2)$$

The distance between two subsequent vectors is defined as the Chebychev distance (Kløve, 2011), which is the absolute value of the elements between these two subsequent vectors:

$$Dis[\Psi_i^m, \Psi_j^m] = max_{k=1,2,\dots m} |H_{i+k} - H_{j+k}| ,$$
(3a)

$$\Psi_i^m = \{H_i, H_{i+1} \dots H_{i+m-1}\},\ \Psi_j^m = \{H_j, H_{j+1} \dots H_{j+m-1}\} \quad 1 \le i, j \le N - m, i \ne j. \quad (3b)$$

To verify the similarity of two subsequent vectors, the recommended criterion is based on the standard deviation of the original time series (Richman & Moorman, 2000; Delgado-Bonal & Marshak, 2019):

$$B_{i,j}^m = \begin{cases} 1 & when\ Dis[\Psi_i^m, \Psi_j^m] \le r \times std(H) \\ 0 & when\ Dis[\Psi_i^m, \Psi_j^m] > r \times std(H) \end{cases} \quad 1 \le i, j \le N - m, i \ne j, \quad (4)$$

where $r \times std(H)$ is a tolerance to determine whether two subsequent vectors are similar. Then the numbers of similar vectors in the subsequent matrix are calculated by:

$$B^m = \frac{1}{2} \sum_{i=1}^{N-m} \sum_{j=1}^{N-m} B_{i,j}^m \qquad 1 \le i, j \le N - m, i \ne j. \quad (5)$$

Next, Ψ^{m+1} is defined as another subsequent matrix of H:

$$\Psi^{m+1} = \begin{bmatrix} H_1 & H_2 & \dots & H_{m+1} \\ H_2 & H_3 & \dots & H_{m+2} \\ \dots & \dots & \dots & \dots \\ H_{N-m} & H_{N-m+1} & \dots & H_n \end{bmatrix}, \quad (6)$$

whose number of columns is $m+1$ and row is $N-m$. The subsequent vector of Ψ^{m+1} is defined as one row in Ψ^{m+1}:

$$\Psi_i^{m+1} = \{H_i, H_{i+1} \dots H_{i+m}\} \quad 1 \le i \le N-m. \quad (7)$$

Similarly, B^{m+1} can be calculated by Ψ^{m+1}:

$$B^{m+1} = \frac{1}{2}\sum_{i=1}^{N-m}\sum_{j=1}^{N-m} B_{i,j}^{m+1} \quad ,$$

(8a)

$$B_{i,j}^{m+1} = \begin{cases} 1 & when\ Dis\left[\Psi_i^{m+1}, \Psi_j^{m+1}\right] \le r \times std(H) \\ 0 & when\ Dis\left[\Psi_i^{m+1}, \Psi_j^{m+1}\right] > r \times std(H) \end{cases} \quad 1 \le i,j \le N-m, i \ne j \quad .$$

(8b)

Finally, SamEn is defined as the proportion of similar numbers between subsequence matrixes Ψ_m and Ψ_{m+1}:

$$SamEn(m,r) = -\ln\left(\frac{B^m}{B^{m+1}}\right). \quad (9)$$

For three-dimensional geophysical variables, such as SSTA (x, y, t) (x represents the longitude, y represents the latitude, and t represents the days), the SamEn of the time series can be calculated in one single grid point, and get the spatial pattern of the SamEn of SSTA.

3 Results and Discussion

3.1 Parameter determination for SamEn

The meridional mean SamEn values of SSTA between 1994 and 2015 are investigated using different parameter values to validate the effect of parameters m, r in the calculation of SamEn (Fig.1). The typical values of m and r are between $[2, 4]$ and $[0.2, 0.4]$ following the previous studies (Ramdani et al., 2009; Zhao et al., 2015; Yin et al., 2020). The value of SamEn is not considerably affected by changing the m values. The absolute values of SamEn fall as r increases, but the relative patterns of SamEn remain the same. The varied factors will not affect the results since only the relative values of SamEn matter. As a result, the SamEn values in this investigation were calculated using $m = 2, r = 0.3$.

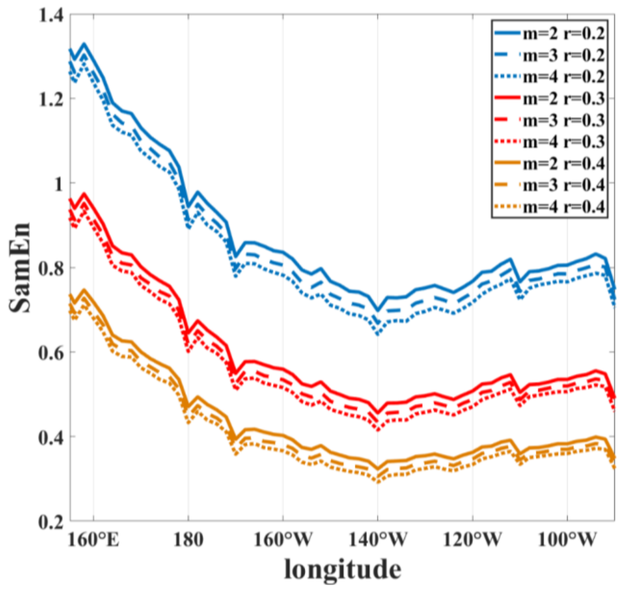

Figure 1. The meridional mean of SamEn value of SSTA between 1994 to 2015 using different parameters ($\boldsymbol{m = [2, 3, 4]}$, $\boldsymbol{r = [0.2, 0.3, 0.4]}$).

3.2 Temporal variation of SamEn

Figure 2 shows the monthly SamEn values in Niño 3 (5°N-5°S, 150°W-90°W), Niño3.4 (5°N-5°S, 170°E-120°W) and Niño 4 (5°N-5°S, 160°E-150°W) regions. Distinct annual cycles can be observed in all three regions. The SamEn value in the Niño 3 region starts to increase in January, peaks in April with a maximum value of 0.78, and decreases thereafter. The average value equals 0.54. The temporal variation of SamEn in the Niño 3.4 region is comparable to that in Niño 3 with a slightly lower average value of 0.51. The SamEn value in Niño 4 region also starts to increase in January, but peaks in May with a maximum value of 0.74 and decays afterward. Considering the abovementioned definition of SamEn, the highest degree of chaos exists in spring in the Niño 3 and 3.4 regions and early summer in the Niño 4 region, which are consistent with the known spring PB of SSTA in the Niño 3 and 3.4 regions (Duan & Wei, 2013), and the early summer PB in the Niño 4 region (Ren et al., 2016; Hou et al., 2019). The more chaotic the air-sea coupled system is, the faster the dynamical model's initial error rises, leading to prediction failure and the PB phenomenon. As a result, monthly fluctuations in the chaotic degree of the air-sea coupled system may be responsible for the known seasonal PB of SSTA in these three locales.

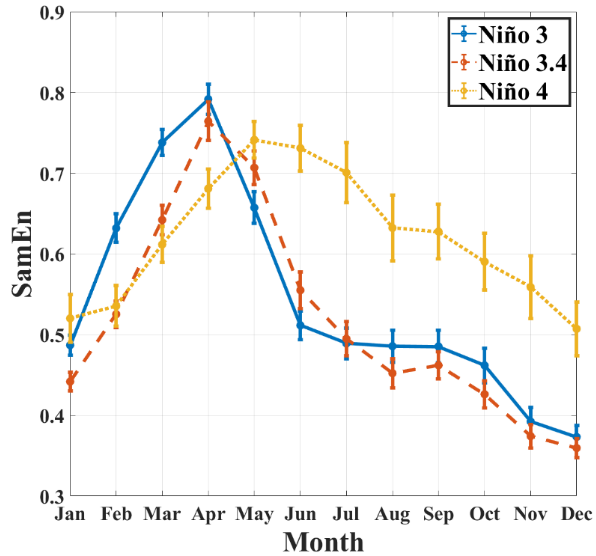

Figure 2. The monthly sample entropy values (SamEn) of SSTA in the Niño 3, Niño 3.4, and Niño 4 regions. Error bars represent the 95% confidence interval.

3.3 Spatial variation of SamEn and PB

Although the temporal variation of the PB in TPO has been extensively investigated in recent decades (Duan & Wei, 2013; Duan & Wu, 2015; Ren et al., 2016), the spatial pattern of PB is less well known (Yu & Kao, 2007). The chaotic characteristic of SSTA is investigated as a function of spatial coordinates (i.e., longitude) in the TPO region using the sample entropy approach. Fig. 3a shows the spatial pattern of the months when the SamEn values peak. The peak months in the eastern TPO are primarily between March and May; in the central TPO, it is mainly in May and June; and in the western TPO, the peak month is after July and exhibits significant spatial variations. The contour plot of the SSTA SamEn values averaged between 5°S-5°N as a function of longitude coordinates and months is shown in Fig. 3b. From 180° E to 100° W, a linear trend of the peak month and the longitude may be observed. The peak month moves later as the coordinates shift westward. This result reveals that the chaotic signal might originate in the eastern TPO during spring, and spread westward to the central TPO. Furthermore, the average SamEn value decreases as it proceeds from the eastern to the central TPO.

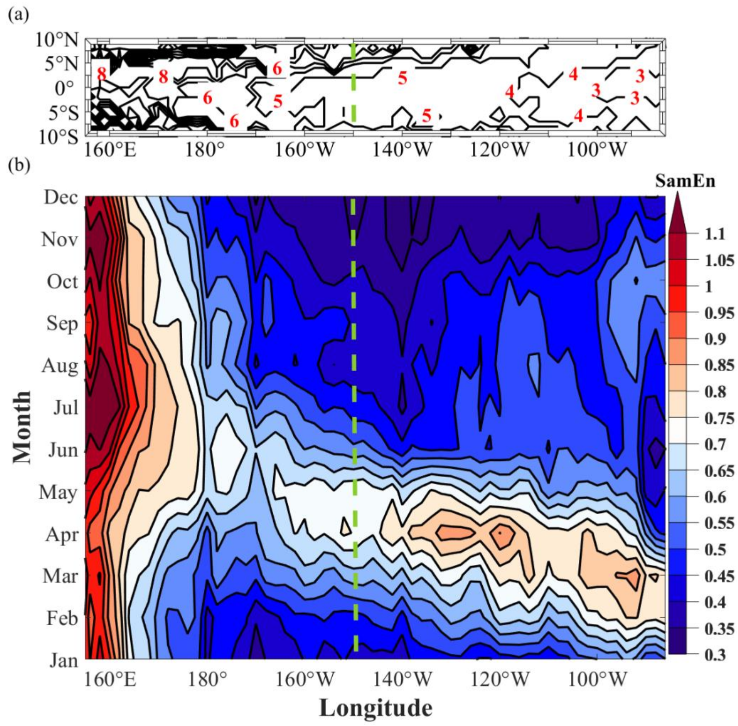

Figure 3. **(a) Contour plot of the month when the sample entropy has the maximum value, the red number represents the peak month; (b) Contour plot of sample entropy value as a function of longitude and month. The data are averaged between 5° S and 5° N. The green dashed line represents the 150°W longitude line, which marks the border between eastern and central TPOs, based on the Niño 3 and Niño 4 regions.**

To link the chaotic degree and the timing of the PB with the forecasting ability, the forecast errors are examined in the NMME dataset, which are defined as the difference between the forecast SSTA value in the NMME data set and the observed SSTA value in the HYCOM data, starting from January. In Fig. 4, the lead time when forecast errors start to grow rapidly shows a linear variation along the longitude, which is near in March and April in the eastern TPO and June and July in the central TPO. The evolution of forecast errors starting from other months displays similar results (More details can be seen in Figure S1). The spatial variation of forecasting ability is compatible with the fluctuation of the SamEn value, indicating another evidence showing that the chaotic regime of the air-sea coupled system could be responsible for the PB phenomenon.

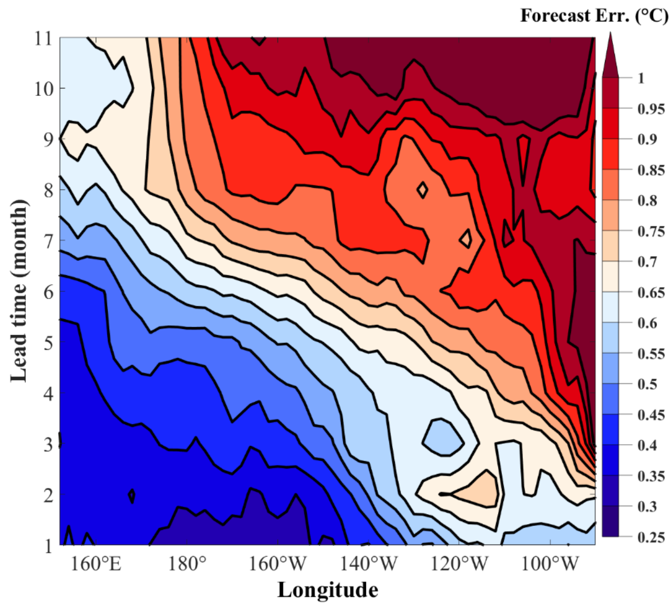

Figure 4. Contour plot of the forecast errors as a function of longitude and lead time, the data are averaged between 5°S and 5°N. The forecast error is computed by the difference between the forecast SSTA value in the NMME dataset and the observed one in the HYCOM dataset. The lead time represents the time after the initial forecast.

5 Conclusions

In this paper, the sample entropy method was utilized to investigate the nonlinear relationship between the predictability barrier of SST anomaly and the air-sea coupled system in the tropical pacific based on the HYCOM reanalysis data and NMME forecast model data.

The meridional mean of the SamEn value of SSTA in the TPO is computed to examine the robustness of the SamEn method with different parameters. When the parameters m and r were adjusted, the variations of the SamEn value remained the same.

On the monthly scale, the degree of chaos was found to peak in April in Niño 3 and Niño 3.4 regions, May, and June in Niño 4 region, which agree with the known spring PB in Niño 3 and Niño 3.4 regions and summer PB in Niño 4 region. In these peak months, the air-sea coupled system is more chaotic, in other words, the initial errors will grow faster and finally result in the corresponding seasonal PB of SSTA. This result indicates that the seasonal variations of the chaotic characteristics of the air-sea coupled system are likely a cause of the PB of SSTA, and the known seasonal initial errors growth of SSTA in these regions may not depend on models but is an intrinsic property. To overcome the PB of SSTA in future dynamic forecasting, more efforts need to be paid to improve the accuracy of SSTA initial fields, especially when the models are initiated in March-June.

We further investigate the monthly variation of the chaotic characteristic averaged between 5°S-5°N along the longitude in the TPO. We found that the most chaotic month increases linearly from March to June as the longitude moves westward. The time when forecast errors firstly quickly grow (i.e., PB timing) also has a similar linear variation along the longitude in the real-time NMME forecast experiment, which indicates another evidence showing that the chaotic regime of the air-sea coupled system could be responsible for the PB phenomenon. The SamEn method can be used to determine the PB timing in the TPO. To the best of our knowledge, it is the first time that the linear variation of PB timing along the longitude in the TPO is found. In the future, taking the TPO as an entire region instead of separate box regions such as Niño 3 and Niño 3.4 may be a better choice to study the PB of SSTA in the TPO.

It is unknown which physical mechanisms cause the nonlinear regime variation of the air-sea couple system. Previous researches have shown that the seasonal variations in tropical background state may play a key role in the spring PB in the eastern TPO (Torrence & Webster, 1998; Mu et al., 2007; Levine & McPhaden, 2015; Larson & Kirtman, 2017; Tian et al., 2019), but few studies have looked at the PB across the TPO. In the future, the dynamic model will be used to further investigate the physical processes leading to the seasonal variation of the nonlinear regime in tropical background states across the entire TPO.

Open Research

The data used to reproduce the results of this paper are located at http://apdrc.soest.hawaii.edu/dods/public_ofes/HYCOM/GLBv0.08 for HYCOM reanalysis data, and http://iridl.ldeo.columbia.edu/SOURCES/.Models/.NMME/ for NMME forecast model data.

References:

Battisti, D. S., & Hirst, A. C. (1989). Interannual variability in a tropical atmosphere-ocean model: influence of the basic state, ocean geometry and nonlinearity. *Journal of the Atmospheric Sciences, 46*(12), 1687–1712. https://doi.org/10.1175/15200469(1989)046<1687:IVIATA>2.0.CO;2

Barnston, A. G., Tippett, M. K., Ranganathan, M., & L'Heureux, M. L. (2019). Deterministic skill of ENSO predictions from the North American Multimodel Ensemble. *Climate Dynamics, 53*(12), 7215–7234. https://doi.org/10.1007/s00382-017-3603-3

Becker, E., Kirtman, B. P., & Pegion, K. (2020). Evolution of the North American Multi-Model Ensemble. *Geophysical Research Letters*, *47*(9), 1–9. https://doi.org/10.1029/2020GL087408

Bradley, E., & Kantz, H. (2015). Nonlinear time-series analysis revisited. *Chaos: An Interdisciplinary Journal of Nonlinear Science, 25*(9), 097610. https://doi.org/10.1063/1.4917289

Castro, C. L., McKee, T. B., & Pielke, R. A. (2001). The relationship of the North American Monsoon to tropical and North Pacific Sea surface temperatures as revealed by observational analyses. *Journal of Climate*, *14*(24), 4449–4473. https://doi.org/10.1175/1520-0442(2001)014<4449:TROTNA>2.0.CO;2

Chassignet, E. P., Hurlburt, H. E., Smedstad, O. M., Halliwell, G. R., Hogan, P. J., Wallcraft, A. J., Baraille, R., & Bleck, R. (2007). The HYCOM (HYbrid Coordinate Ocean Model) data assimilative system. *Journal of Marine Systems*, *65*(1-4 SPEC. ISS.), 60–83. https://doi.org/10.1016/j.jmarsys.2005.09.016

Chen, D., & Cane, M. A. (2008). El Niño prediction and predictability. *Journal of Computational Physics*, *227*(7), 3625–3640. https://doi.org/10.1016/j.jcp.2007.05.014

Chen, D., Cane, M. A., Kaplan, A., Zebiak, S. E., & Huang, D. (2004). Predictability of El Niño over the past 148 years. *Nature*, *428*(6984), 733–736. https://doi.org/10.1038/nature02439

Clancy, R., Bitz, C., & Blanchard-Wrigglesworth, E. (2021). The influence of ENSO on Arctic sea ice in large ensembles and observations. *Journal of Climate*, *34*(24), 9585–9604. https://doi.org/10.1175/jcli-d-20-0958.1

Collins, M., Frame, D., Sinha, B., & Wilson, C. (2002). How far ahead could we predict El Niño?. *Geophysical Research Letters*, *29*(10), 130–1. https://doi.org/10.1029/2001GL013919

Dash, M. K., Pandey, P. C., Vyas, N. K., & Turner, J. (2013). Variability in the ENSO-induced southern hemispheric circulation and Antarctic sea ice extent. *International Journal of Climatology*, *33*(3), 778–783. https://doi.org/10.1002/joc.3456

Delgado-Bonal, A., & Marshak, A. (2019). Approximate entropy and sample entropy: A comprehensive tutorial. *Entropy*, *21*(6), 1–37. https://doi.org/10.3390/e21060541

Ding, R., & Li, J. Nonlinear finite-time Lyapunov exponent and predictability. *Physics Letters A*, *364*(5), 396–400. https://doi.org/10.1016/j.physleta.2006.11.094

Duan, W., & Wei, C. (2013). The “spring predictability barrier” for ENSO predictions and its possible mechanism: Results from a fully coupled model. *International Journal of Climatology*, *33*(5), 1280–1292. https://doi.org/10.1002/joc.3513

Duan, W., & Wu, Y. (2015). Season-dependent predictability and error growth dynamics of Pacific Decadal Oscillation-related sea surface temperature anomalies. *Climate Dynamics*, *44*(3–4), 1053–1072. https://doi.org/10.1007/s00382-014-2364-5

Eduardo Virgilio Silva, L., & Otavio Murta, L. (2012). Evaluation of physiologic complexity in time series using generalized sample entropy and surrogate data analysis. *Chaos*, *22*(4), 043105. https://doi.org/10.1063/1.4758815

Fereday, D. R., Knight, J. R., Scaife, A. A., Folland, C. K., & Philipp, A. (2008). Cluster analysis of North Atlantic-European circulation types and links with tropical Pacific Sea surface temperatures. *Journal of Climate*, *21*(15), 3687–3703. https://doi.org/10.1175/2007JCLI1875.1

Fraedrich, K. (1987). Estimating weather and climate predictability on attractors. *Journal of the Atmospheric Sciences*, *44*(4), 722–728. https://doi.org/10.1175/15200469(1987)044<0722:EWACPO>2.0.CO;2

Gao, H., Wang, Y., & He, J. (2006). Weakening significance of ENSO as a predictor of summer precipitation in China. *Geophysical Research Letters*, *33*(9). https://doi.org/10.1029/2005GL025511

Hou, M., Duan, W., & Zhi, X. (2019). Season-dependent predictability barrier for two types of El Niño revealed by an approach to data analysis for predictability. *Climate Dynamics*, *53*(9–10), 5561–5581. https://doi.org/10.1007/s00382-019-04888-w

Hu, Q., & Feng, S. (2012). AMO- and ENSO-driven summertime circulation and precipitation variations in North America. *Journal of Climate*, *25*(19), 6477–6495. https://doi.org/10.1175/JCLI-D-11-00520.1

Hu, S., Fedorov, A. V., Lengaigne, M., & Guilyardi, E. (2014). The impact of westerly wind bursts on the diversity and predictability of El Niño events: An ocean energetics perspective. *Geophysical Research Letters*, *41*(13), 4654–4663. https://doi.org/10.1002/2014GL059573

Hua, L., D.-Z. Sun, and Y. Yu, (2019). Why Do We Have El Niño: Quantifying A Diabatic and Nonlinear Perspective Using Observations. *Climate Dynamics*, *52*(11), 6705-6717. https://doi.org/10.1007/s00382-018-4541-4

Infanti, J. M., & Kirtman, B. P. (2016). North American rainfall and temperature prediction response to the diversity of ENSO. *Climate Dynamics*, *46*(9–10), 3007–3023. https://doi.org/10.1007/s00382-015-2749-0

Jin, F. F. (1997). An equatorial ocean recharge paradigm for ENSO. Part II: A stripped-down coupled model. *Journal of the Atmospheric Sciences*, *54*(7), 830–847. https://doi.org/10.1175/15200469(1997)054<0830:AEORPF>2.0.CO;2

Jin, E. K., Kinter, J. L., Wang, B., Park, C. K., Kang, I. S., Kirtman, B. P., Kug, J. S., Kumar, A., Luo, J. J., Schemm, J., Shukla, J., & Yamagata, T. (2008). Current status of ENSO prediction skill in coupled ocean-atmosphere models. *Climate Dynamics*, *31*(6), 647–664. https://doi.org/10.1007/s00382-008-0397-3

Kantz, H., & Schreiber, T. (2004). *Nonlinear time series analysis* (Vol. 7). Cambridge university press.

Karamperidou, C., Cane, M. A., Lall, U., & Wittenberg, A. T. (2014). Intrinsic modulation of ENSO predictability viewed through a local Lyapunov lens. *Climate Dynamics*, *42*(1–2), 253–270. https://doi.org/10.1007/s00382-013-1759-z

Katok, A. (1980). Lyapunov exponents, entropy and periodic orbits for diffeomorphisms. *Publications Mathématiques de L'Institut Des Hautes Scientifiques*, *51*(1), 137–173. https://doi.org/10.1007/BF02684777

Kim, I. (2021). Multiscale sample entropy of two-dimensional decaying turbulence. *Entropy*, *23*(2), 1–9. https://doi.org/10.3390/e23020245

Kirtman, B. P., & Min, D. (2009). Multimodel ensemble ENSO prediction with CCSM and CFS. *Monthly Weather Review*, *137*(9), 2908–2930. https://doi.org/10.1175/2009MWR2672.1

Kirtman, B. P., Min, D., Infanti, J. M., Kinter, J. L., Paolino, D. A., Zhang, Q., Van Den Dool, H., Saha, S., Mendez, M. P., Becker, E., Peng, P., Tripp, P., Huang, J., Dewitt, D. G., Tippett, M. K., Barnston, A. G., Li, S., Rosati, A., Schubert, S. D., … Wood, E. F. (2014). The North American multimodel ensemble: Phase-1 seasonal-to-interannual prediction; phase-2 toward developing intraseasonal prediction. *Bulletin of the American Meteorological Society*, *95*(4), 585–601. https://doi.org/10.1175/BAMS-D-12-00050.1

Kløve, T. (2011). Lower bounds on the size of spheres of permutations under the Chebychev distance. *Designs, Codes and Cryptography*, *59*(1), 183-191.

Lake, D. E., Richman, J. S., Pamela Griffin, M., & Randall Moorman, J. (2002). Sample entropy analysis of neonatal heart rate variability. *American Journal of Physiology - Regulatory Integrative and Comparative Physiology*, *283*(3 52-3), 789-797. https://doi.org/10.1152/ajpregu.00069.2002

Larson, S. M., & Kirtman, B. P. (2015). An alternate approach to ensemble ENSO forecast spread: Application to the 2014 forecast. *Geophysical Research Letters*, *42*(21), 9411–9415. https://doi.org/10.1002/2015GL066173

Larson, S. M., & Kirtman, B. P. (2017). Drivers of coupled model ENSO error dynamics and the spring predictability barrier. *Climate Dynamics*, *48*(11–12), 3631–3644. https://doi.org/10.1007/s00382-016-3290-5

Lau, K. M., & Yang, S. (1996). The Asian monsoon and predictability of the tropical ocean-atmosphere system. *Quarterly Journal of the Royal Meteorological Society*, *122*(532), 945–957. https://doi.org/10.1256/smsqj.53207

Levine, A. F. Z., & McPhaden, M. J. (2015). The annual cycle in ENSO growth rate as a cause of the spring predictability barrier. *Geophysical Research Letters*, *42*(12), 5034–5041. https://doi.org/10.1002/2015GL064309

Li, C., & Ling, J. (2009). Physical Essence of the “Predictability Barrier.” *Atmospheric and Oceanic Science Letters*, *2*(5), 290–294. https://doi.org/10.1080/16742834.2009.11446810

Li, J., & Ding, R. (2013). Temporal-spatial distribution of the predictability limit of monthly sea surface temperature in the global oceans. *International Journal of Climatology*, *33*(8), 1936–1947. https://doi.org/10.1002/joc.3562

Li, Y., Chen, X., Yu, J., Yang, X., & Yang, H. (2019). The data-driven optimization method and its application in feature extraction of ship-radiated noise with sample entropy. *Energies*, *12*(3). https://doi.org/10.3390/en12030359

Lin, H., Merryfield, W. J., Muncaster, R., Smith, G. C., Markovic, M., Dupont, F., Roy, F., Lemieux, J. F., Dirkson, A., Kharin, V. V., Lee, W. S., Charron, M., & Erfani, A. (2020). The canadian seasonal to interannual prediction system version 2 (Cansipsv2). *Weather and Forecasting*, *35*(4), 1317–1343. https://doi.org/10.1175/WAF-D-19-0259.1

Liang, J., X.-Q. Yang, and D.-Z. Sun, 2012: The effect of ENSO events on the Tropical Pacific Mean Climate: Insights from an Analytical Model. *Journal of Climate*, *25*(21), 7590–7606. https://doi.org/10.1175/JCLI-D-11-00490.1

Liang, J., X.-Q. Yang, and D.-Z. Sun, 2017: Factors Determining the Asymmetry of ENSO. *Journal of Climate*, *30*(16), 6097-6106. https://doi.org/10.1175/JCLI-D-16-0923

Liu, D., Duan, W., Feng, R., & Tang, Y. (2018). Summer Predictability Barrier of Indian Ocean Dipole Events and Corresponding Error Growth Dynamics. *Journal of Geophysical Research: Oceans*, *123*(5), 3635–3650. https://doi.org/10.1029/2017JC013739

Lopez, H., & Kirtman, B. P. (2014). WWBs, ENSO predictability, the spring barrier and extreme events. *Journal of Geophysical Research*, *119*(17), 10–114. https://doi.org/10.1002/2014JD021908

Lorenz E N. (1963). Deterministic nonperiodic flow. *Journal of atmospheric sciences, 20*(2), 130–141. https://doi.org/10.1175/1520-0469(1963)020<0130:DNF>2.0.CO;2

Marzban, C., & Schaefer, J. T. (2001). The correlation between U.S. tornadoes and pacific sea surface temperatures. *Monthly Weather Review*, *129*(4), 884–895. https://doi.org/10.1175/1520-0493(2001)129<0884:TCBUST>2.0.CO;2

McKinnon, K. A., Rhines, A., Tingley, M. P., & Huybers, P. (2016). Long-lead predictions of eastern United States hot days from Pacific sea surface temperatures. *Nature Geoscience*, *9*(5), 389–394. https://doi.org/10.1038/ngeo2687

McPhaden, M. J. (2003). Tropical Pacific Ocean heat content variations and ENSO persistence barriers. *Geophysical Research Letters*, *30*(9). https://doi.org/10.1029/2003GL016872

Moore, A. M. (1999). The dynamics of error growth and predictability in a model of the Gulf Stream. Part II: Ensemble prediction. *Journal of Physical Oceanography*, *29*(4), 762–778. https://doi.org/10.1175/1520-0485(1999)029<0762:TDOEGA>2.0.CO;2

Mukhin, D., Gavrilov, A., Seleznev, A., & Buyanova, M. (2021). An Atmospheric Signal Lowering the Spring Predictability Barrier in Statistical ENSO Forecasts. *Geophysical Research Letters*, *48*(6), 1–10. https://doi.org/10.1029/2020GL091287

Mu, M., Duan, W., & Wang, B. (2007). Season-dependent dynamics of nonlinear optimal error growth and El Niño-Southern Oscillation predictability in a theoretical model. *Journal of Geophysical Research Atmospheres, 112*(10). https://doi.org/10.1029/2005JD006981

Patt, A., & Gwata, C. (2002). Effective seasonal climate forecast applications: Examining constraints for subsistence farmers in Zimbabwe. *Global Environmental Change*, *12*(3), 185–195. https://doi.org/10.1016/S0959-3780(02)00013-4

Pierce W., D. W. (2002). The role of sea surface temperatures in interactions between ENSO and the North Pacific Oscillation. *Journal of Climate*, *15*(11), 1295–1308. https://doi.org/10.1175/1520-0442(2002)015<1295:trosst>2.0.co;2

Pincus, S. (1995). Approximate entropy (ApEn) as a complexity measure. *Chaos*, *5*(1), 110–117. https://doi.org/10.1063/1.166092

Pincus, S. (1991). Approximate entropy as a measure of system complexity. *Proceedings of the National Academy of Sciences*, *88*(6), 2297–2301.

Ramdani, S., Seigle, B., Lagarde, J., Bouchara, F., & Bernard, P. L. (2009). On the use of sample entropy to analyze human postural sway data. *Medical Engineering and Physics*, *31*(8), 1023–1031. https://doi.org/10.1016/j.medengphy.2009.06.004

Ren, H. L., Jin, F. F., Tian, B., & Scaife, A. A. (2016). Distinct persistence barriers in two types of ENSO. *Geophysical Research Letters*, *43*(20), 10,973-10,979. https://doi.org/10.1002/2016GL071015

Richman, J. S., & Moorman, J. R. (2000). Physiological time-series analysis using approximate entropy and sample entropy maturity in premature infants Physiological time-series analysis using approximate entropy and sample entropy. *Americal Journal of Physiology Heart and Circulatory Physiology*, *278*(6), H2039–H2049.

Ropelewski, C. F., & Halpert, M. S. (1986). North American precipitation and temperature patterns associated with the El Nino/Southern Oscillation (ENSO). *Monthly Weather Review*, *114*(12), 2352–2362. https://doi.org/10.1175/15200493(1986)114<2352:NAPATP>2.0.CO;2

Samelson, R. M., & Tziperman, E. (2001). Instability of the chaotic ENSO: The growth-phase predictability barrier. *Journal of the Atmospheric Sciences*, *58*(23), 3613–3625. https://doi.org/10.1175/1520-0469(2001)058<3613:IOTCET>2.0.CO;2

Schneider, T., Bischoff, T., & Haug, G. H. (2014). Migrations and dynamics of the intertropical convergence zone. *Nature*, *513*(7516), 45–53. https://doi.org/10.1038/nature13636

Shannon, C. E. (1948). A mathematical theory of communication. *The Bell system technical journal*, 27(3), 379-423.

Shi, W., & Shang, P. (2013). Cross-sample entropy statistic as a measure of synchronism and cross-correlation of stock markets. *Nonlinear Dynamics, 71*(3), 539–554. https://doi.org/10.1007/s11071-012-0680-z

Solow, A. R., Adams, R. F., Bryant, K. J., Legler, D. M., O'Brien, J. J., McCarl, B. A., Nayda, W., & Weiher, R. (1998). The value of improved ENSO prediction to U.S. Agriculture. *Climatic Change*, *39*(1), 47–60. https://doi.org/10.1023/A:1005342500057

Song, Y., Zhao, Y., Yin, X., Bao, Y., & Qiao, F. (2020). Evaluation of FIO-ESM v1.0 Seasonal Prediction Skills Over the North Pacific. *Frontiers in Marine Science*, *7*, 504. https://doi.org/10.3389/fmars.2020.00504

Strogatz, S.H. (2015). Lorenz Equation. *Nonlinear Dynamics and Chaos: With Applications to Physics, Biology, Chemistry, and Engineering (2nd ed.)* (pp.329). CRC Press. Chapter 9 page 329 https://doi.org/10.1201/9780429492563

Sun, D.-Z. (1997). El Niño: a coupled response to radiative heating? *Geophysical Research Letters*, *24*(16), 2031-2034. https://doi.org/10.1029/97GL01960

Tang, Y., Zhang, R. H., Liu, T., Duan, W., Yang, D., Zheng, F., Ren, H., Lian, T., Gao, C., Chen, D., & Mu, M. (2018). Progress in ENSO prediction and predictability study. *National Science Review*, *5*(6), 826-839. https://doi.org/10.1093/nsr/nwy105

Tian, B., Ren, H. L., Jin, F. F., & Stuecker, M. F. (2019). Diagnosing the representation and causes of the ENSO persistence barrier in CMIP5 simulations. *Climate Dynamics, 53*(3–4), 2147–2160. https://doi.org/10.1007/s00382-019-04810-4

Torrence, C., & Webster, P J. (1998). The annual cycle of persistence in the El Nino/Southern Oscillation. *Quarterly Journal of the Royal Meteorological Society*, *124*(550), 1985–2004. https://doi.org/10.1256/smsqj.55009

Trenberth, K. E., Branstator, G. W., Karoly, D., Kumar, A., Lau, N. C., & Ropelewski, C. (1998). Progress during TOGA in understanding and modeling global teleconnections associated with tropical sea surface temperatures. *Journal of Geophysical Research: Oceans*, *103*(C7), 14291–14324. https://doi.org/10.1029/97jc01444

van Oldenborgh, G. J., Balmaseda, M. A., Ferranti, L., Stockdale, T. N., & Anderson, D. L. T. (2005). Did the ECMWF seasonal forecast model outperform statistical ENSO forecast models over the last 15 years? *Journal of Climate*, *18*(16), 3240–3249. https://doi.org/10.1175/JCLI3420.1

Waliser, D. E., & Gautier, C. (1993). A satellite-derived climatology of the ITCZ. *Journal of climate*, *6*(11), 2162-2174. https://doi.org/10.1175/15200442(1993)006<2162:ASDCOT>2.0.CO;2

Wang, H., & Ting, M. (2000). Covariabilities of winter U.S. precipitation and Pacific Sea surface temperatures. *Journal of Climate*, *13*(20), 3711–3719. https://doi.org/10.1175/15200442(2000)013<3711:COWUSP>2.0.CO;2

Webster, P J. (1995). The annual cycle and the predictability of the tropical coupled ocean-atmosphere system. *Meteorology and Atmospheric Physics*, *56*(1–2), 33–55. https://doi.org/10.1007/BF01022520

Webster, Peter J., & Yang, S. (1992). Monsoon and Enso: Selectively Interactive Systems. *Quarterly Journal of the Royal Meteorological Society*, *118*(507), 877–926. https://doi.org/10.1002/qj.49711850705

Wolff, R. C. L. (1992). Local Lyapunov Exponents: Looking Closely at Chaos. *Journal of the Royal Statistical Society: Series B (Methodological)*, *54*(2), 353–371. https://doi.org/10.1111/j.2517-6161.1992.tb01886.x

Wu, R., Hu, Z. Z., & Kirtman, B. P. (2003). Evolution of ENSO-related rainfall anomalies in East Asia. *Journal of Climate*, *16*(22), 3742–3758. https://doi.org/10.1175/1520-0442(2003)016<3742:EOERAI>2.0.CO;2

Wu, R., Yang, S., Liu, S., Sun, L., Lian, Y., & Gao, Z. (2010). Changes in the relationship between Northeast China summer temperature and ENSO. *Journal of Geophysical Research Atmospheres*, *115*(21). https://doi.org/10.1029/2010JD014422

Xue, Y., Chen, M., Kumar, A., Hu, Z. Z., & Wang, W. (2013). Prediction skill and bias of tropical pacific sea surface temperatures in the NCEP climate forecast system version 2. *Journal of Climate*, *26*(15), 5358–5378. https://doi.org/10.1175/JCLI-D-12-00600.1

Yin, J., Xiao, P. X., Li, J., Liu, Y., Yan, C., & Zhang, Y. (2020). Parameters Analysis of Sample Entropy, Permutation Entropy and Permutation Ratio Entropy for RR Interval Time Series. *Information Processing and Management*, *57*(5). https://doi.org/10.1016/j.ipm.2020.102283

Yu, J. Y., & Kao, H. Y. (2007). Decadal changes of ENSO persistence barrier in SST and ocean heat content indices: 1958-2001. *Journal of Geophysical Research Atmospheres*, *112*(13), 1–10. https://doi.org/10.1029/2006JD007654

Yu, Y., Duan, W., Xu, H., & Mu, M. (2009). Dynamics of nonlinear error growth and season-dependent predictability of El Niño events in the Zebiak-Cane model. *Quarterly Journal of the Royal Meteorological Society*, *135*(645), 2146–2160. https://doi.org/10.1002/qj.526

Yuan, X. (2004). ENSO-related impacts on Antarctic sea ice: A synthesis of phenomenon and mechanisms. *Antarctic Science*, *16*(4), 415–425. https://doi.org/10.1017/S0954102004002238

Yuan, Y., & Yang, S. (2012). Impacts of different types of El NiñO on the East Asian climate: Focus on ENSO cycles. *Journal of Climate*, *25*(21), 7702–7722. https://doi.org/10.1175/JCLI-D-11-00576.1

Zhao, L., Wei, S., Zhang, C., Zhang, Y., Jiang, X., Liu, F., & Liu, C. (2015). Determination of sample entropy and fuzzy measure entropy parameters for distinguishing congestive heart failure from normal sinus rhythm subjects. *Entropy*, *17*(9), 6270–6288. https://doi.org/10.3390/e17096270

Zheng, F., & Zhu, J. (2010). Spring predictability barrier of ENSO events from the perspective of an ensemble prediction system. *Global and Planetary Change*, *72*(3), 108–117. https://doi.org/10.1016/j.gloplacha.2010.01.021

Geophysical Research Letters

Supporting Information for

A Nonlinear Cause for the seasonal Predictability Barrier of SST anomaly in the tropical Pacific

Dakuan Yu,[1] Meng Zhou,[1] Chaoxun Hang,[1] De-Zheng Sun,[2]

[1] *School of Oceanography, Shanghai Jiao Tong University, Shanghai, China*

[2] *Institute of Atmospheric Sciences, Fudan University, Shanghai, China*

Contents of this file

Introduction

This support information provides additional information from the main article.

Table S1. The NMME model set used in this study. The hindcast data are available for download at the International Research Institute for Climate and Society (IRI) (http://iridl.ldeo.columbia.edu/SOURCES/.Models/.NMME/)

Model name	No. ensemble members	Hindcast period	Reference
CanCM4i	10	1981-2018	Lin et al., 2020
CanSIPSv2	20	1981-2018	Lin et al., 2020
COLA-RSMAS-CCSM3	6	1982-2018	Kirtman & Min, 2009
COLA-RSMAS-CCSM4	10	1982-2021	Kirtman & Min, 2009
GFDL-CM2p5-FLOR-A06	12	1980-2021	Kirtman et al., 2014
GFDL-CM2p5-FLOR-B01	12	1980-2021	Kirtman et al., 2014
GFDL-CM2p1-aer04	10	1982-2021	Kirtman et al., 2014
GEM-NEMO	10	1981-2018	Lin et al., 2020

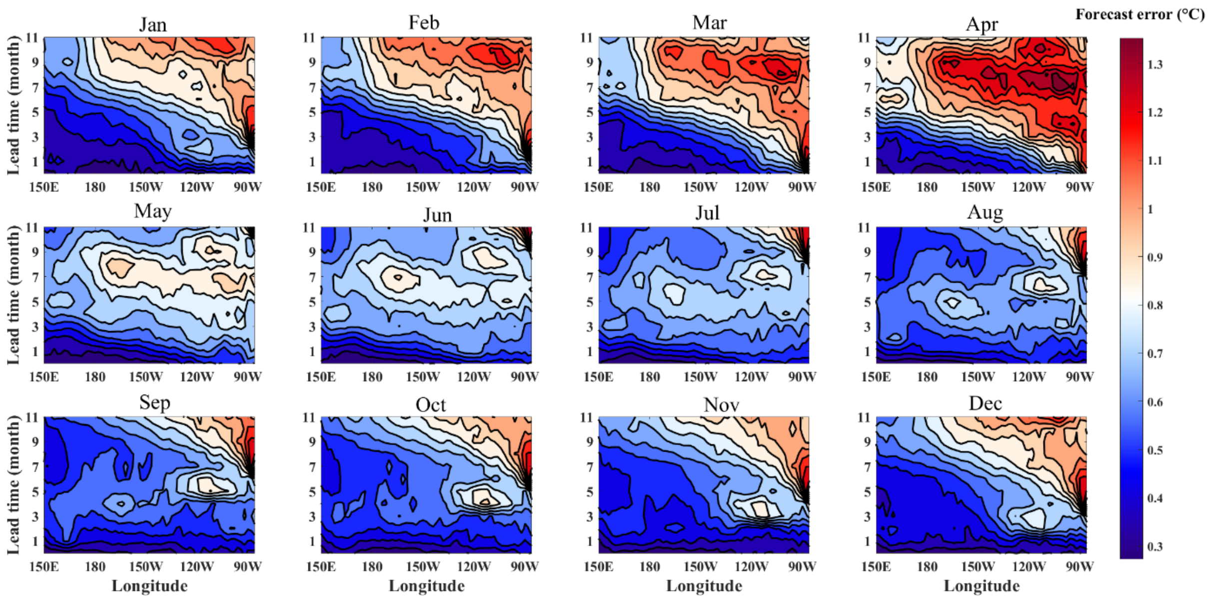

Figure S1. The forecast error of predicted tropical SSTA (averaged within 5°S-5°N) from NMME ensemble hindcasts and forecasts, with the model starting from the different months (vertical coordinate corresponds to varying lead times).